Supporting information

Enhancing cycle performance of MgH_2-$LiBH_4$ based solid-state batteries via stacking pressure tailoring

Xueye Zhuang, Haoliang Chen, Shiman He*, Long Hu, Hui Wang *, and Renzong Hu*

School of Materials Science and Engineering, Guangdong Provincial Key Laboratory of Advanced Energy Storage Materials, South China University of Technology, Guangzhou, 510641, China

*Corresponding author: heshm@scut.edu.cn
mehwang@scut.edu.cn
msrenzonghu@scut.edu.cn

Experimental sections

MgH_2 composite electrodes: MgH_2 (98% purity) was obtained from MG power Corp. First, raw MgH_2 was refined by planetary milling for 10 h at 400 rpm in 1.5 MPa H_2 atmosphere. The MgH_2 composite electrodes were prepared by planetary milling of MgH_2, $LiBH_4$ (95%, Aladdin) and conductive carbon (Super P) with a mass ratio of 1:1:2 at 400 rpm for 10 h.

S cathode: S powder was mixed with carbon nanotubes(CNTs) at a mass ratio of 1:1 and ground for 1 h. Then, the homogeneous mixture was transferred to a tube furnace and heated at 155 ℃ for 12 h and at 200 ℃ for 1 h under argon atmosphere to obtain the S@CNTs. The S cathode was obtained by hand milling S@CNTs, $LiBH_4$, and conductive carbon (Super P) with a mass ratio of 4:4:2 for 1 hour.

All operations were carried out in a glovebox filled with argon gas and the water and oxygen content less than 0.1 ppm.

Material characterization

X-ray diffraction (XRD, PANalytical) was used to determine the phase structure of the materials. Scanning electron microscopy (TESCAN GAIA3 model 2016 UHR) were used to examine the morphology of materials.

Cell assembly and electrochemical tests

The all-solid-state battery was assembled in a battery mold with a pressure sensor. The cell mold is composed of two conductive stainless-steel pistons and a polyetherketone (Peek) cylinder with an inner diameter of 10 mm. Typically, 75 mg of $LiBH_4$ powder was added into the cell mold and pressed at 400 MPa, then 6 mg of MgH_2 electrode material was pressed on one side of the electrolyte, 9.5 mm diameter Li foil were covered on the other side in turn. The symmetric cells were assembled with the same method as all solid-state battery except that the MgH_2 electrode was changed to Li. To equip the Mg-LiH|$LiBH_4$|S all-solid-state lithium battery, a MgH_2||Li half-cell was first discharged to 0.3 V at a current density of 0.05 C. The lithium sheet was then uncovered, poured with 4 mg of S cathode and cold pressed at 400 MPa.

All electrochemical tests were measured at 125 °C to ensure the high ionic conductivity of $LiBH_4$ electrolyte. The Li|$LiBH_4$|MgH_2 ASSBs were galvanostatically

charged and discharged range from 0.3 to 1 V (vs Li^+/Li). The cutoff voltage of 0.3 V could avoid the formation of irreversible LiMg alloys. Mg-LiH|$LiBH_4$|S ASSBs were galvanostatically charged and discharged range from 0.8 to 2.6 V at 0.1 C (1 C= 1672 mAh g^{-1}).

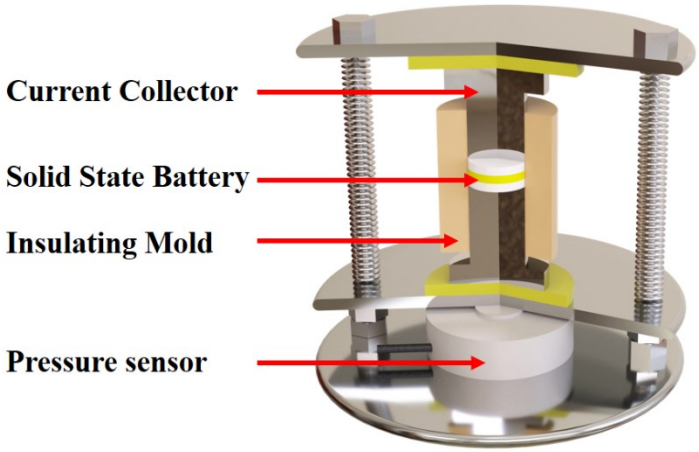

Fig. S1 Schematic diagram of all-solid-state lithium battery with pressure sensor.

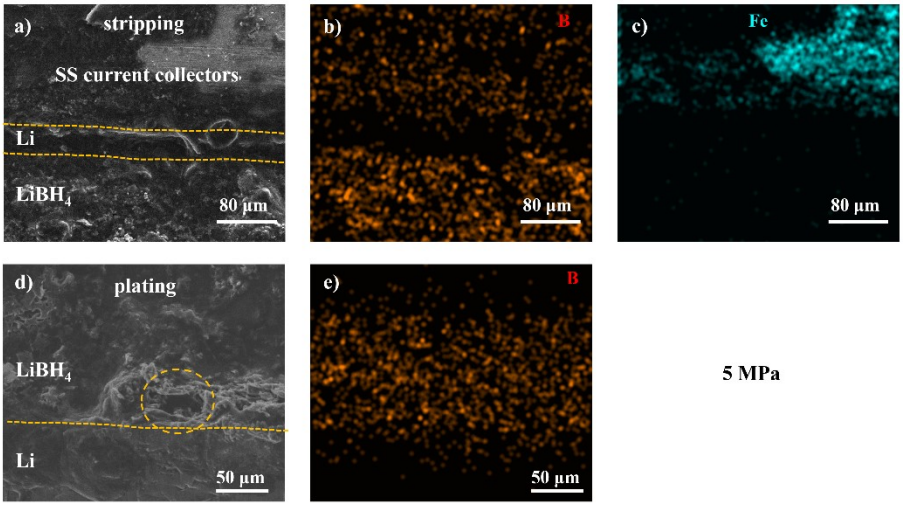

Fig. S2 Cross-sectional SEM image of the $LiBH_4$ electrolyte with 5 MPa and the corresponding EDS mapping: (a-c) stripping state; (d-e) plating state.

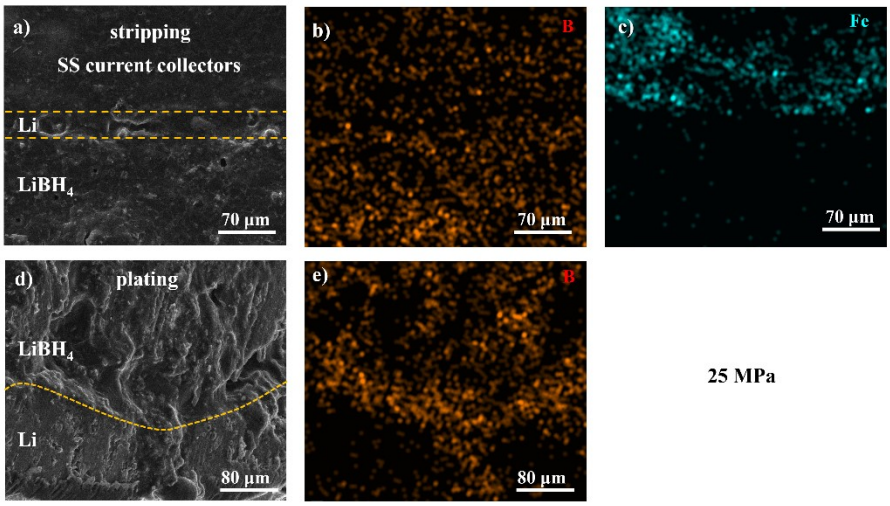

Fig. S3 Cross-sectional SEM image of the $LiBH_4$ electrolyte with 25 MPa and the corresponding EDS mapping: (a-c) stripping state; (d-e) plating state.

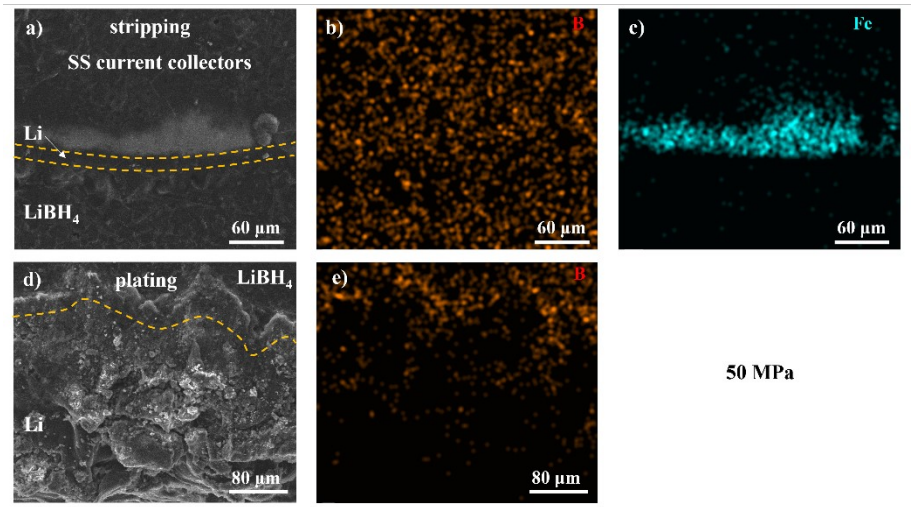

Fig. S4 Cross-sectional SEM image of the $LiBH_4$ electrolyte with 50 MPa and the corresponding EDS mapping: (a-c) stripping state; (d-e) plating state.

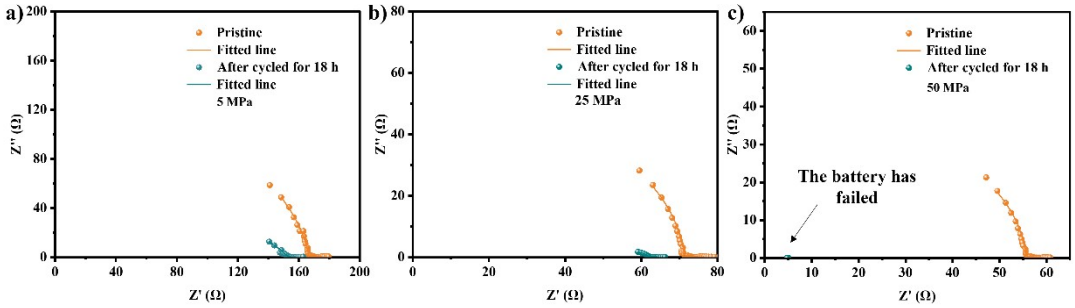

Fig. S5 Electrochemical impedance spectra of the Li|$LiBH_4$|Li cells before and after cycling with different stacking pressure: (a) 5 MPa; (b) 25 MPa and (c) 50 MPa.

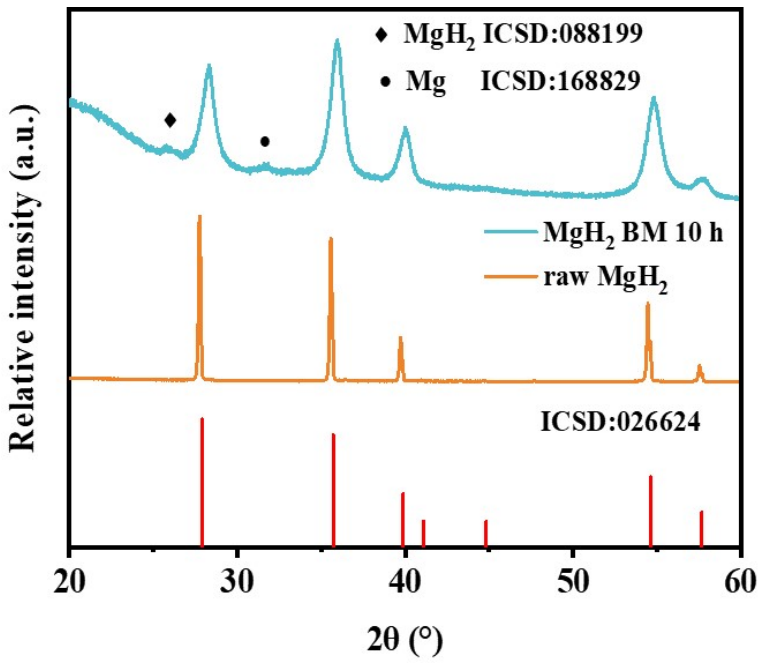

Fig. S6 XRD patterns of raw MgH_2 and MgH_2 after ball milling for 10 h.

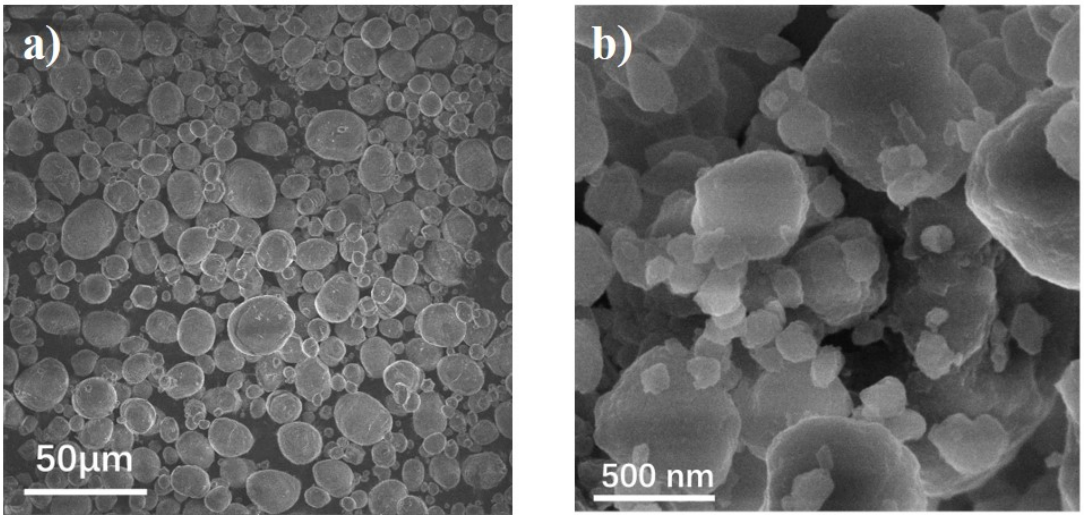

Fig. S7 SEM images of (a) raw MgH_2 and (b) MgH_2 after ball milling for 10 h.

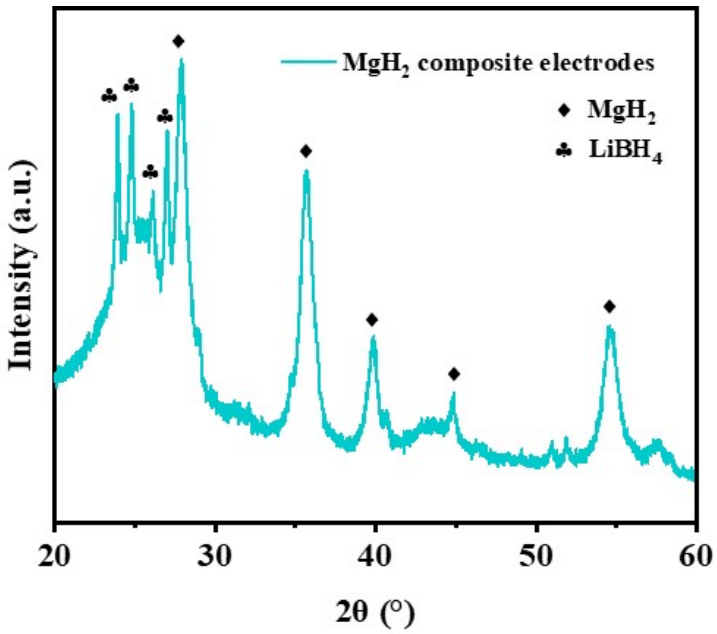

Fig. S8 XRD pattern of MgH_2 composite electrode.

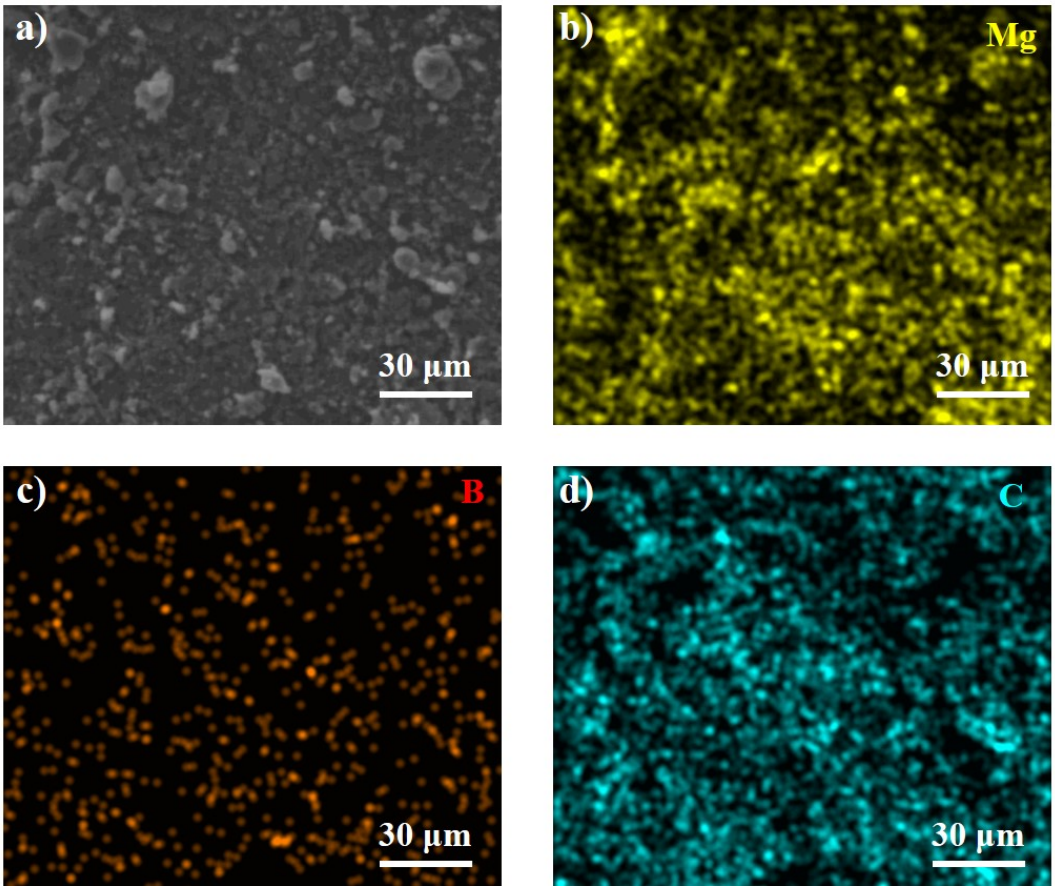

Fig. S9 SEM image and the corresponding EDS mappings of MgH_2 electrode.

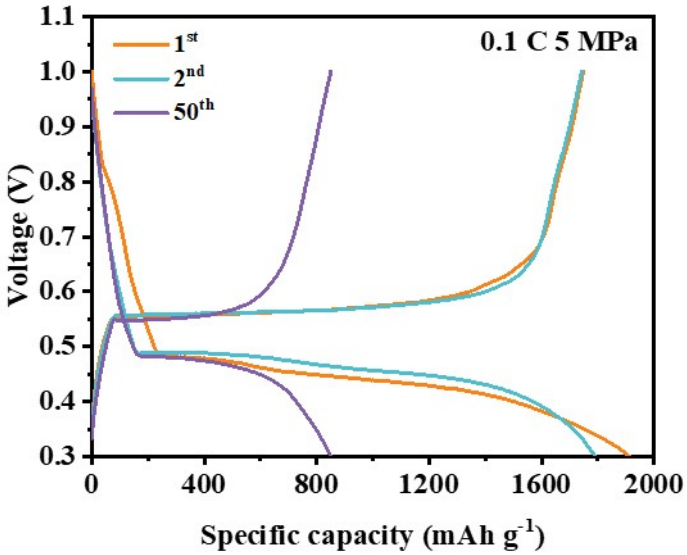

Fig. S10 Galvanostatic charge–discharge profiles of Li|$LiBH_4$|MgH_2 battery with a stacking pressure of 5 MPa at 0.1 C.

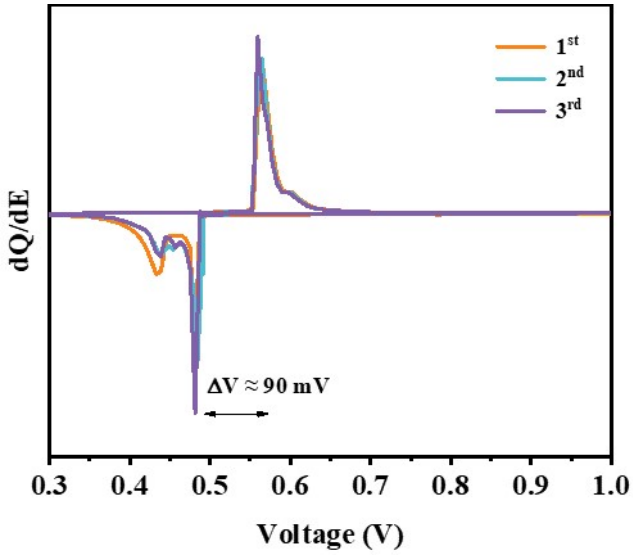

Fig. S11 Derivative curves (dQ/dE) of Li|$LiBH_4$|MgH_2 battery with a stacking pressure of 25 MPa at 0.1 C.

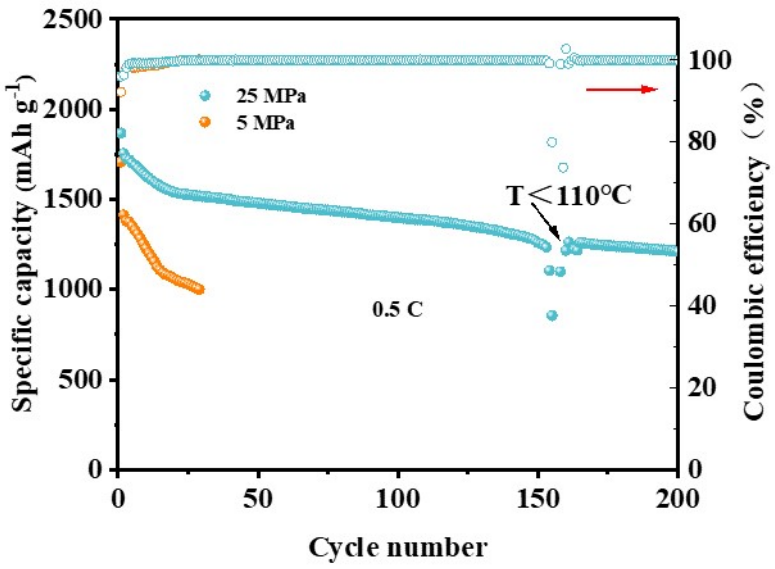

Fig. S12 Cycling performances of the Li|$LiBH_4$|MgH_2 batteries at different stacking pressures at 0.5 C.

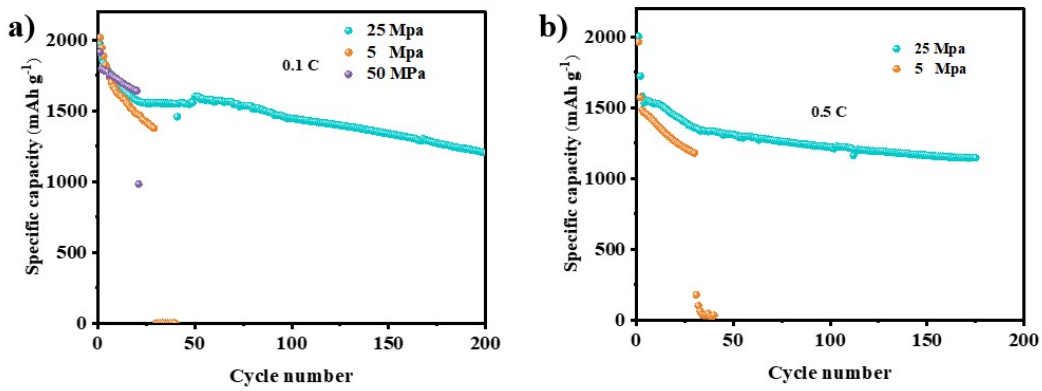

Fig. S13 The repeatability testing of the cycling performances for Li|$LiBH_4$|MgH_2 cells with different pressures at (a) 0.1 C and (b) 0.5 C.

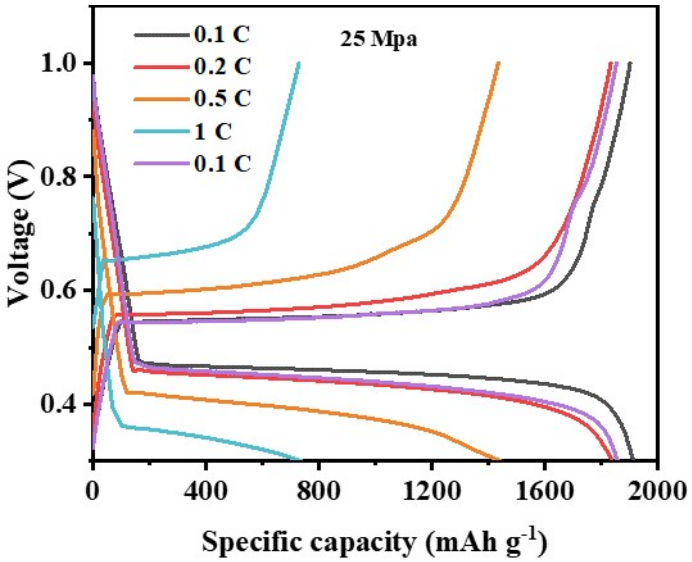

Fig. S14 Galvanostatic charge–discharge profiles of the Li|$LiBH_4$|MgH_2 battery in rate test at 25MPa.

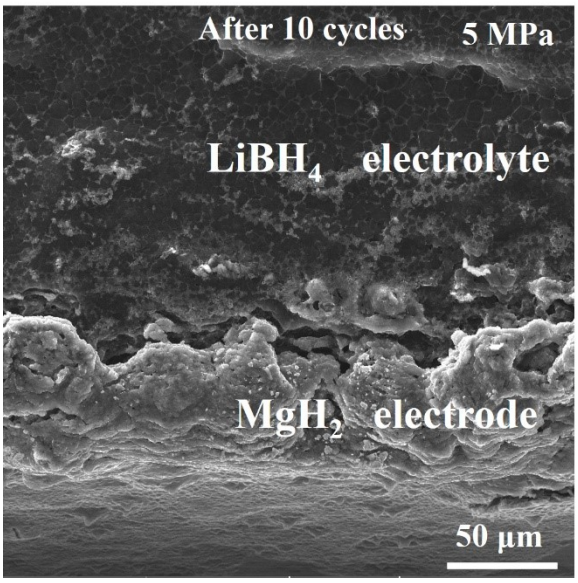

Fig. S15 Cross-sectional SEM images of the interface between MgH_2 and the solid electrolyte after 10 cycles at 5 MPa, 0.1 C.

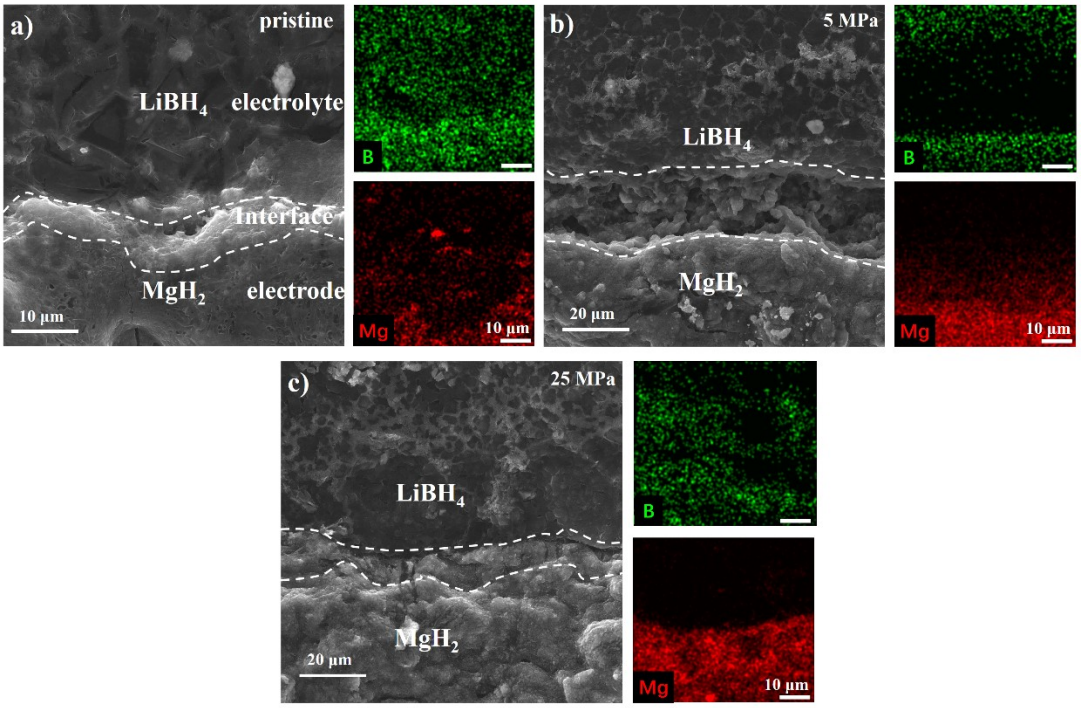

Fig. S16 Cross-sectional SEM images and the corresponding EDS mappings of the interface between MgH_2 and the solid electrolyte: (a) initial state and after 10 cycles at (b) 5 MPa (c)and 25 MPa at 0.1 C.

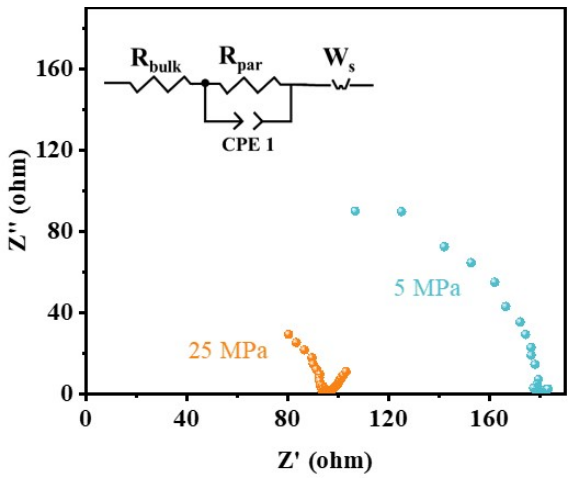

Fig. S17 Electrochemical impedance spectra of Li|$LiBH_4$|MgH_2 batteries at different stacking pressures.

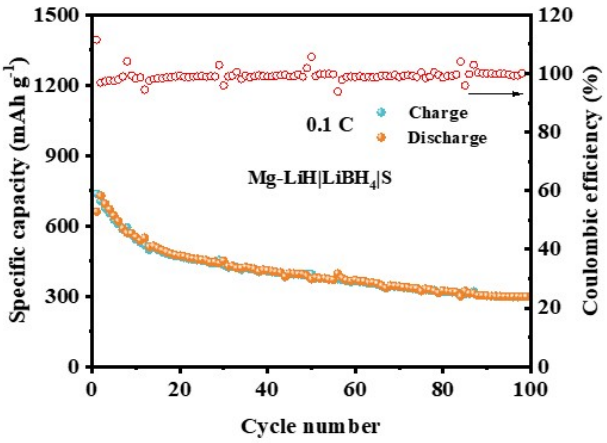

Fig. S18. The repeatability testing of the cycling performances for Mg-LiH|$LiBH_4$|S cell with 25 MPa at 0.1 C.

Table S1. A comparison of the electrochemical properties of our MgH_2 electrodes with the previously reported works.

electrode	Current dengsity(mA g^{-1})	cycle	Capacity retention (mAh g^{-1})	Ref.
MgH_2	203.8	200	1246.2	This wok
	1019	200	1210.2	
MgH_2-Nb_2O_5	800	50	924	1
MgH_2-CoO	67.5	20	910	2
MgH_2-Al_2O_3	200	9	580	3
MgH_2- TiH_2	34	10	865	4
MgH_2-VGCF	1000	50	1221	5
$Nd_4Mg_{80}Ni_8H_x$	203.8	100	1191	6
	2038	100	997	
MgH_2-graphene	100	50	1214	7
	400	200	597	
MgH_2-graphene@$MgBH_4$	200	150	1498	8
	1000	350	1318	

Reference

1 L. Zeng, K. Kawahito, S. Ikeda, T. Ichikawa, H. Miyaoka, Y. Kojima. Chem. Commun (Camb).2015, **51**(48), 9773-9776.

2 A. El Kharbachi, H. Uesato, H. Kawai, S. Wenner, H. Miyaoka, M. H. Sørby, H. Fjellvåg, T. Ichikawa, B. C. Hauback. RSC Adv.2018, **8**(41), 23468-74.

3 T. I. Suguru Ikeda, Kiyotaka Goshome, Shotaro Yamaguchi, Hiroki Miyaoka & Yoshitsugu Kojima J. Solid State Electrochem.2015, 19, (3639–3644).

4 A. H. Dao, N. Berti, P. López-Aranguren, J. Zhang, F. Cuevas, C. Jordy, M. Latroche. J. Power Sources.2018, **397**(143-149).

5 L. Zeng, T. Ichikawa, K. Kawahito, H. Miyaoka, Y. Kojima. ACS Appl Mater Interfaces.2017, **9**(3), 2261-6.

6 P. Gao, S. Ju, Z. Liu, G. Xia, D. Sun, X. Yu. ACS Nano.2022, 16, 8040.

7 Y. Lv, X. Zhang, W. Chen, S. Ju, Z. Liu, G. Xia, T. Ichikawa, T. Zhang, X. Yu. J. Mater. Sci. Technol.2023, **155**(47-53).

8 Y. Huang, P. Gao, T. Zhang, X. Zhang, G. Xia, F. Fang, D. Sun, Z. Guo, X. Yu. Small.2023, **19**(26), e2207210.